Electromagnetically induced transparency in an open multilevel system

Tian Li, Mei-Ju Lu, and Jonathan D. Weinstein

Phys. Rev. A **84**, 023801 — Published 1 August 2011

DOI: 10.1103/PhysRevA.84.023801

Electromagnetically-induced transparency in an open multilevel system

Tian Li, Mei-Ju Lu, and Jonathan D. Weinstein*

Department of Physics, University of Nevada, Reno NV 89557, USA

Abstract

Electromagnetically-induced transparency in a multilevel system is investigated in ^{173}Yb. The level structure investigated is "open" in that the light that gives rise to the transparency also resonantly couples the atoms to excited states which do not exhibit electromagnetically-induced transparency. The resulting reduction of transparency is investigated experimentally and theoretically. It is found that, while the transparency is poor in certain regimes, it can be made to perform arbitrarily well in the limit of a large intensity imbalance between the optical fields.

PACS numbers: 42.50.Gy, 32.80.Qk, 42.65.-k

* weinstein@physics.unr.edu; http://www.physics.unr.edu/xap/

I. INTRODUCTION

The technique of electromagnetically-induced transparency (EIT) has become of great interest due to its potential to create strong, coherent coupling between light and atomic ensembles [1]. It has potential applications in quantum communication and quantum information [2, 3].

The basic theory of EIT is often described in terms of an ideal three-level "lambda" system, but EIT is most commonly implemented in atoms with a much larger number of levels. Studies of the consequences of multilevel structure have explored the effects of Zeeman degeneracy on EIT [4–6] as well as EIT in "chain lambda" systems [7]. It was found that for "closed" multilevel systems (i.e. systems that exhibited true dark states) the multilevel system could be mapped onto a three-level system [8]. EIT in a multilevel cascade system has been investigated for the case in which all the cascade systems share a common ground-state level [9]. Applications of closed multilevel systems for phase gates [10] and quantum memory [11] have also been explored. In addition, the reduction of STIRAP transfer efficiency due to multiple intermediate levels has been investigated [12]. Open multilevel systems (often referred to as N-type sytems), in which an additional light field resonantly couples one leg of the lambda transition to an excited state which can spontaneously decay, have been analyzed for their potential applications in nonlinear interactions [13–15].

In this work, we examine EIT in an open multilevel system, in which the same beams that give rise to the EIT through multiple coupled lambda systems also resonantly couple the atoms to a state that gives rise to scattering. We examine the reduction in transparency due to this coupling, and calculate how the behavior depends on the number of coupled lambda systems involved.

While the theoretical results we obtain are general to such open systems, we specifically consider the ${}^1S_0\ F = 5/2 \rightarrow {}^1\ P_1\ F' = 5/2$ transition of the ^{173}Yb atom, shown in Fig 1. Here, the EIT arises because of coherence between the nuclear spin states of the electronic ground state of ^{173}Yb; this system has been shown to be a favorable environment for light storage due to the slow decoherence of the nuclear spin states [17]. Here, we analyze the limitations due to its open structure.

We first analyze this system with a simple toy model. We then calculate the steady-state light scattering properties from the density matrix. Finally, we compare the theory to

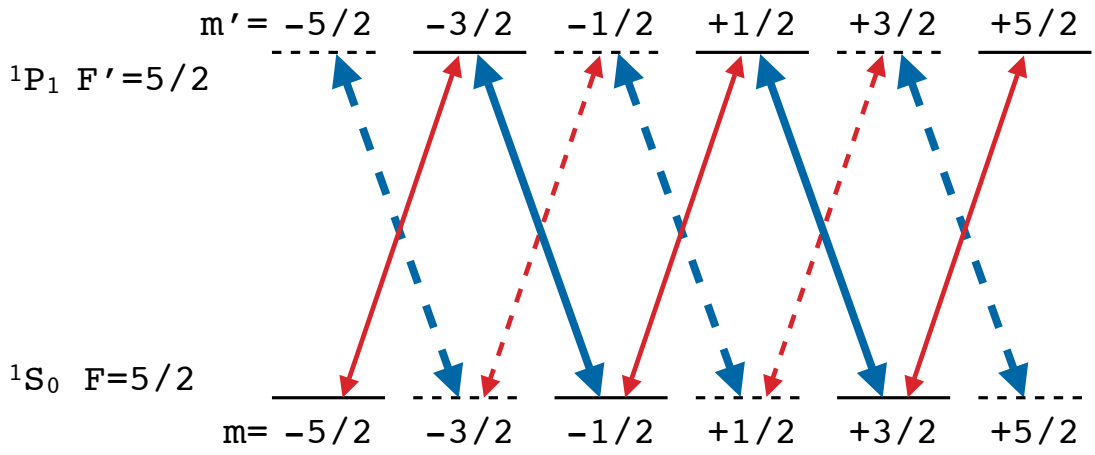

FIG. 1. (Color online) Relevant level structure of ^{173}Yb, shown with a strong σ_- control beam (thick blue arrows) and a weak σ_+ probe beam (thin red arrows). The $F' = 3/2$ and $F' = 7/2$ excited-state hyperfine lines (not shown) lie 737 MHz and 821 MHz above the $F' = 5/2$ level, respectively [16]. The m_F states with dashed lines are coupled to each other through the control and probe beams, as are the states with solid lines. The dashed states couple to the solid states only through spontaneous emission.

experimental measurements.

II. TOY MODEL

As seen in Figure 1, there is no true dark state for the $F = 5/2 \rightarrow F' = 5/2$ transition in ^{173}Yb. However, in the limit that the control beam intensity is much higher than the probe beam intensity, an approximate dark state exists. A superposition of the $m = -\frac{5}{2}$, $-\frac{1}{2}$, and $+\frac{3}{2}$ states can be created such that the different excitation paths to the $m' = -\frac{3}{2}$ and $+\frac{1}{2}$ states interfere destructively, preventing scattering. Only excitation to the $m' = +\frac{5}{2}$ will remain, but in the limit of a weak probe beam, the resulting scattering rate will be small.

In the ideal three-level lambda-type system, illustrated in Figure 2, the dark state is $|\Psi_{dark}\rangle = \cos(\theta)|a\rangle - \sin(\theta)|b\rangle$, where $\left|\frac{\cos(\theta)}{\sin(\theta)}\right| = \frac{\Omega_b}{\Omega_a}$ [18]. If P_a and P_b are the probabilities of finding the atom in states a and b, respectively, and I_a and I_b are the intensities of the two coupling beams, then when the atom is in the dark state $\frac{P_a}{P_b} = \frac{I_b}{I_a}$.

For a transition such as shown in Figure 1, with an even number n of ground-state

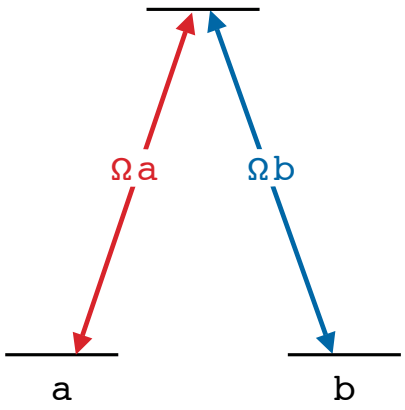

FIG. 2. (Color online) A three-level system, with couplings of Rabi frequencies Ω_a and Ω_b.

and excited state levels, we have $(n-2)/2$ coupled 3-level systems. If we assume that $I_p \ll I_c$ and I_p is weak compared to the saturation intensity, then — for the "quasidark" state — the probability of finding the atom in the m state with the "leak" is $\propto R^{(n-2)/2}$, where we define R as the ratio of the intensities of the weak beam to that of the strong beam (here, $R = I_p/I_c$). Hence the scattering rate out of the quasidark state will scale as $\gamma_{dark} \propto I_p \cdot R^{(n-2)/2}$.

If, upon scattering, the atom does not decay back into the quasidark state, it will continue scattering photons until it does. We expect that the scattering rate while the atom remains in this "bright" state will scale as $\gamma_{bright} \propto I_c$. As we assume that $I_c \gg I_p$, the atom will spend the majority of its time in the quasidark state.

For a fixed atomic density, the absorption coefficient α is proportional to the scattering rate per atom divided by the intensity. Hence the absorption coefficient for the probe beam should scale as

$$\alpha_p \propto \gamma_{dark}/I_p \propto R^{(n-2)/2} \tag{1}$$

For the probe beam driving the $F = 5/2 \rightarrow F' = 5/2$ transition of ^{173}Yb, this is a scaling of $OD \propto R^2$.

For the strong coupling beam, we scatter photons at a rate proportional to the weak beam scattering rate: once the atom scatters out of the quasidark state, it will scatter a few control beam photons before returning to it. Due to the power differences in the two beams,

we expect

$$\frac{\alpha_c}{\alpha_p} \propto R \tag{2}$$

Hence, for ^{173}Yb, we expect $\alpha_c \propto R^3$

III. THEORY

While the toy model provides the scaling in the limit of a large intensity imbalance, it does not provide a quantitative prediction of the scattering, nor does it predict the transparency outside of this limiting case. To obtain this information, we use the density matrix to calculate the steady-state scattering rate.

A. Interaction picture and the density matrix

The Schrödinger equation of the atom in the presence of the driving fields can be written as

$$\frac{d}{dt}|\Psi(t)\rangle = -i\hat{H}(t)|\Psi(t)\rangle \tag{3}$$

where $|\Psi(t)\rangle$ is the state of the atom and $\hat{H}(t)$ is the total Hamiltonian. The Planck constant $\hbar$ has been set to be one. For an atom with n ground-state and excited-state Zeeman sublevels, $|\Psi(t)\rangle$ can expanded by a complete and orthogonal set of state vectors $|\psi_k\rangle$:

$$|\Psi(t)\rangle = \sum_{k=1}^{2n} C_k(t)|\psi_k\rangle \text{ and } \sum_{k=1}^{2n} |\psi_k\rangle\langle\psi_k| = 1 \tag{4}$$

where $C_k(t)$ is a time-dependent parameter, satisfying $\sum_{k=1}^{2n} |C_k(t)|^2 = 1$. We choose $k = 1, 2, \cdots, n$ to denote the Zeeman sublevels of the ground state F, and $k = n+1, n+2, \cdots, 2n$ denote the Zeeman sublevels of the excited state F'. The total Hamiltonian $\hat{H}(t)$ is a composition of the Hamiltonian $\hat{H}_0$ of a bare atom and the atom-field interaction $\hat{H}_1(t)$:

$$\hat{H}(t) = \hat{H}_0 + \hat{H}_1(t) \tag{5}$$

The Hamiltonian of the bare atom $\hat{H}_0$ is written as

$$\hat{H}_0 = \sum_{k=1}^{2n} \omega_k |\psi_k\rangle\langle\psi_k| \tag{6}$$

where ω_k is the angular frequency of the corresponding energy level. Here, $\omega_k = 0$ for the ground-state Zeeman sublevels and $\omega_k = \omega_0$ for the excited-state Zeeman sublevels, where ω_0 is the atomic resonance frequency. The atom-field interaction term can be presented under the dipole approximation:

$$\hat{H}_1(t) = -\hat{\vec{\mu}} \cdot \vec{E}_c \cos(\omega_c t) - \hat{\vec{\mu}} \cdot \vec{E}_p \cos(\omega_p t) \tag{7}$$

where $\omega_{c,p}$ are the angular frequencies of the control and probe beam, respectively. The Rabi frequencies of the probe and control beams are $\Omega_{p,c} = \mu|\vec{E}_{p,c}|$, respectively, and μ is the corresponding dipole matrix element. In the case of a σ^+-polarized probe beam and a σ^--polarized control beam, the atom-field interaction is given by

$$\begin{aligned} \hat{H}_1(t) = &-\frac{\Omega_p}{2}(e^{-it\omega_p} + e^{it\omega_p}) \sum_{k=1}^{n-1} |\psi_k\rangle\langle\psi_{k+n+1}| \\ &-\frac{\Omega_c}{2}(e^{-it\omega_c} + e^{it\omega_c}) \sum_{k=2}^{n} |\psi_k\rangle\langle\psi_{k+n-1}| \end{aligned} \tag{8}$$

where the relative phase between these fields has set to zero, without loss of generality. In Eq.(8), we have assumed the allowed transitions all have equal strength for simplicy. Later, when we simulate the level structure of ^{173}Yb, the relative strengths of the different transitions are included.

To simplify Eq. (8) we apply the rotating wave approximation. We first use a unitary operator $\hat{U}(t)$ to transform the time base of Eq.(3), while still keeps the same physical properties. The operator $\hat{U}(t) = e^{-it\hat{G}}$ satisfies that

$$\hat{U}^\dagger(t)\hat{U}(t) = \hat{U}(t)\hat{U}^\dagger(t) = \mathbf{1} \tag{9}$$

$\hat{U}(t)$ and $\hat{G}$ are both Hermitian and commute with each other. The matrix element of $\hat{U}(t)$ can be written as $U_{kl} = e^{-itu_k}\delta_{kl}$, and that of $\hat{G}$ is $G_{kl} = u_k\delta_{kl}$. δ_{kl} is the Kronecker delta and $k, l = 1, 2, \cdots, 2n$. In this way, $|\Psi(t)\rangle$ is transformed to $|\Psi_I(t)\rangle$ by

$$|\Psi_I(t)\rangle = \hat{U}^\dagger(t)|\Psi(t)\rangle \tag{10}$$

$$= \sum_{k=1}^{2n} C_k(t) e^{itu_k} |\psi_k\rangle \tag{11}$$

The time derivative of $|\Psi_I(t)\rangle$ can be written in a form similar to Eq.(3) by defining an

effective Hamiltonian:

$$\frac{d}{dt}|\Psi_I(t)\rangle = (-i)\hat{U}^\dagger(t)(-\hat{G}+\hat{H}(t))\hat{U}(t)|\Psi_I(t)\rangle \tag{12}$$

$$= (-i)\hat{H}_{\text{eff}}(t)|\Psi_I(t)\rangle \tag{13}$$

$\hat{H}_{\text{eff}}$ is determined by the chosen $\hat{U}(t)$ in a way that the $e^{\pm it\omega_{c,p}}$ terms in Eq.(8) becomes either static or fast oscillating. Consequently, the parameters u_k of $\hat{U}(t)$ obey the following relations:

$$u_{k+n+1} - u_k = \omega_p \ , \ \text{for } k = 1, 2, \cdots, n-1 \tag{14}$$

$$u_{k+n-1} - u_k = \omega_c \ , \ \text{for } k = 2, 3, \cdots, n \tag{15}$$

These relations are obtained by plugging Eg.(3) into the time derivative of $|\Psi_I(t)\rangle$ and rewrite it in the form of Eq.(13). For $n \geq 2$, the other parameters are determined based on Eq.(14) and Eg.(15) after choosing $u_1 = u_2 = 0$. We also define the frequency detunings as

$$\begin{aligned} \Delta_1 &= \omega_0 - \omega_p \\ \Delta_2 &= \omega_0 - \omega_c \\ \delta &= \Delta_1 - \Delta_2 \end{aligned} \tag{16}$$

Positive $\Delta_{1,2}$ refers to the red frequency detuning, and δ is the two-photon detuning. An example of $\hat{H}_{\text{eff}}$ for the $n = 4$ case is shown in Eq.(17).

$$\hat{H}_{\text{eff}} = \begin{pmatrix} 0 & 0 & 0 & 0 & 0 & -\frac{\Omega_p}{2} & 0 & 0 \\ 0 & 0 & 0 & 0 & -\frac{\Omega_c}{2} & 0 & -\frac{\Omega_p}{2} & 0 \\ 0 & 0 & \delta & 0 & 0 & -\frac{\Omega_c}{2} & 0 & -\frac{\Omega_p}{2} \\ 0 & 0 & 0 & \delta & 0 & 0 & -\frac{\Omega_c}{2} & 0 \\ 0 & -\frac{\Omega_c}{2} & 0 & 0 & \Delta_2 & 0 & 0 & 0 \\ -\frac{\Omega_p}{2} & 0 & -\frac{\Omega_c}{2} & 0 & 0 & \Delta_1 & 0 & 0 \\ 0 & -\frac{\Omega_p}{2} & 0 & -\frac{\Omega_c}{2} & 0 & 0 & \Delta_1 & 0 \\ 0 & 0 & -\frac{\Omega_p}{2} & 0 & 0 & 0 & 0 & \delta + \Delta_1 \end{pmatrix} \tag{17}$$

The ensemble average of the system is evaluated by the density matrix, $\hat{\rho}_I(t) = |\Psi_I(t)\rangle\langle\Psi_I(t)|$. According to the Liouville equation [19, 20], we write the equation of motion in the interaction picture as

$$\frac{d\hat{\rho}_I(t)}{dt} = -i[\hat{H}_{\text{eff}}, \hat{\rho}_I(t)] - \frac{1}{2}(\hat{\Gamma}\hat{\rho}_I(t) + \hat{\rho}_I(t)\hat{\Gamma}) - \hat{\Lambda} \tag{18}$$

where we have added terms on the right-hand side of Eq.(18) to account for spontaneous decay: $\hat{\Gamma}$ is a relaxation matrix with the excited-state decay rate γ, and $\hat{\Lambda}$ is a repopulation matrix [20]. With both $\hat{\Gamma}$ and $\hat{\Lambda}$, we ensure the population is conserved. We take the $n = 4$ system as an example, and show the matrix forms of $\hat{\Gamma}$ and $\hat{\Lambda}$ in Eq.(21) and Eq.(22). Again, we have assumed all allowed transitions are of the same strength for simplicity.

We calculate the steady-state solution of the density matrix from the equations:

$$\sum_{k,l=1}^{2n} \frac{d}{dt}\hat{\rho}_{kl}(t) = 0 \text{ and } \sum_{k=1}^{2n} \hat{\rho}_{kk}(t) = 1. \tag{19}$$

where the $\hat{\rho}_{kl}$ are the density matrix elements of the density matrix operator $\hat{\rho}_I(t)$ in the interaction picture and rotating-wave frame.

The absorption coefficient α of the probe beam passing through the Yb EIT medium is given by the imaginary part of these density matrix elements [18, 19]:

$$\alpha_{\text{probe}} = \alpha_0 \sum_{k=1}^{n-1} \mathbf{Im}[\hat{\rho}_{k,k+n+1}]/\Omega_p \tag{20}$$

where α_0 is the absorption coefficient without the presence of EIT and the saturation effect.

$$\hat{\Gamma} = \begin{pmatrix} 0 & 0 & 0 & 0 & 0 & 0 & 0 & 0 \\ 0 & 0 & 0 & 0 & 0 & 0 & 0 & 0 \\ 0 & 0 & 0 & 0 & 0 & 0 & 0 & 0 \\ 0 & 0 & 0 & 0 & 0 & 0 & 0 & 0 \\ 0 & 0 & 0 & 0 & \gamma & 0 & 0 & 0 \\ 0 & 0 & 0 & 0 & 0 & \gamma & 0 & 0 \\ 0 & 0 & 0 & 0 & 0 & 0 & \gamma & 0 \\ 0 & 0 & 0 & 0 & 0 & 0 & 0 & \gamma \end{pmatrix} \tag{21}$$

$$\hat{\Lambda} = \begin{pmatrix} -\frac{\gamma\rho_{5,5}}{2} - \frac{\gamma\rho_{6,6}}{3} & 0 & 0 & 0 & 0 & 0 & 0 & 0 \\ 0 & -\frac{\gamma\rho_{5,5}}{2} - \frac{\gamma\rho_{6,6}}{3} - \frac{\gamma\rho_{7,7}}{3} & 0 & 0 & 0 & 0 & 0 & 0 \\ 0 & 0 & -\frac{\gamma\rho_{6,6}}{3} - \frac{\gamma\rho_{7,7}}{3} - \frac{\gamma\rho_{8,8}}{2} & 0 & 0 & 0 & 0 & 0 \\ 0 & 0 & 0 & -\frac{\gamma\rho_{7,7}}{3} - \frac{\gamma\rho_{8,8}}{2} & 0 & 0 & 0 & 0 \\ 0 & 0 & 0 & 0 & 0 & 0 & 0 & 0 \\ 0 & 0 & 0 & 0 & 0 & 0 & 0 & 0 \\ 0 & 0 & 0 & 0 & 0 & 0 & 0 & 0 \\ 0 & 0 & 0 & 0 & 0 & 0 & 0 & 0 \end{pmatrix} \tag{22}$$

B. Simulations

The calculated absorption coefficient is shown in Figure 3 for the cases of $n = 4$ and $n = 6$. We model the EIT medium as an ensemble of atoms with no Doppler or pressure broadening. We note that — in the limit that the light intensity is $\ll$ the saturation intensity — α/α_0 is independent of the single-photon detuning, so — for collinear beams — the graph would be unchanged by the inclusion of Doppler broadening.

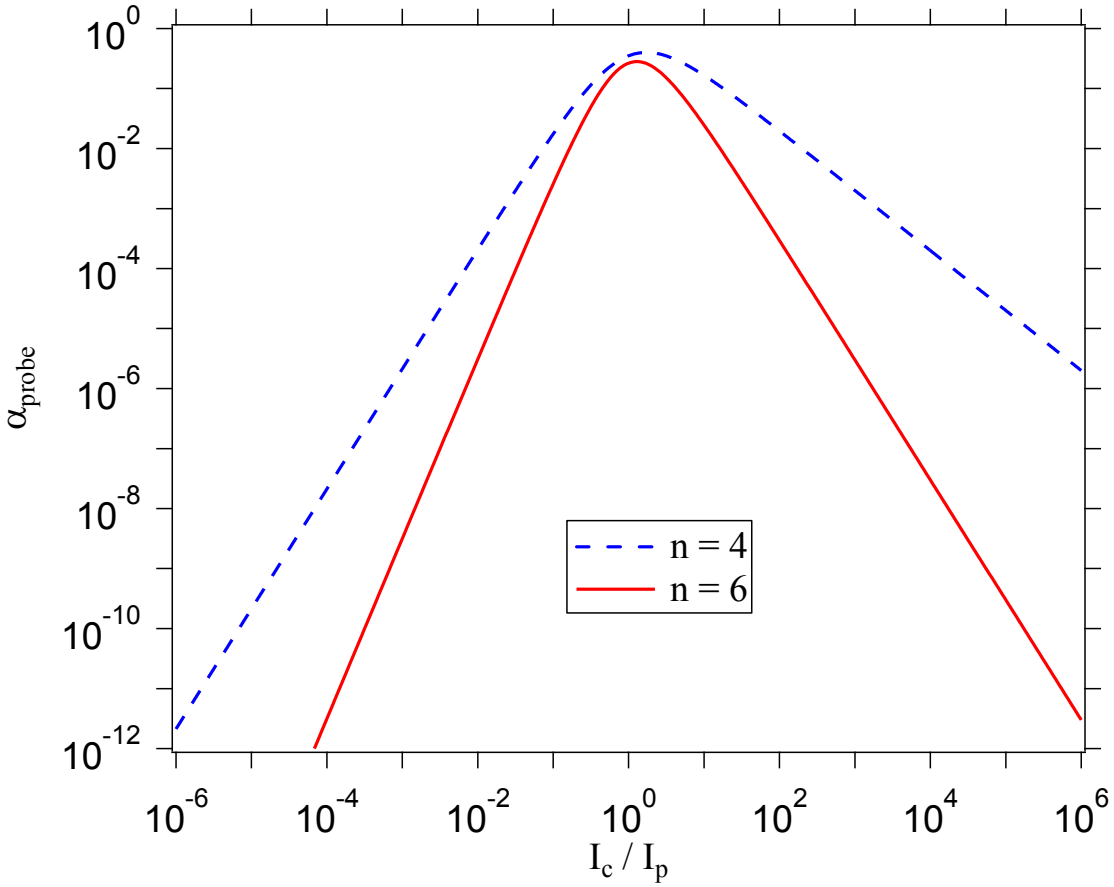

FIG. 3. (Color online) The calculated absorption coefficient as a function of the intensity ratio of the beams, for $n = 4$ and $n = 6$ atoms. Calculated in the limit that $\Omega_p, \Omega_c \ll \gamma$, with $\Delta_1 = \Delta_2 = 0$, with the assumption that all transitions were of the same strength. The absorption coefficient is normalized such that $\alpha = 1$ in the absence of EIT and saturation. For $n = 3$ and $n = 5$, $\alpha_{\text{probe}} = 0$ for all values of I_p/Ic. This is because of the closed level structure for odd n.

In the limit of large intensity ratios, the expected asymptotic behavior is observed: the

absorption coefficient is proportional to $R^{(n-2)/2}$ for the weak beam (right-hand side of Fig. 3) and $R^{n/2}$ for the strong beam (left-hand side of Fig. 3).

We repeated the calculation for the $n = 6$ case using the actual relative transition strengths of ^{173}Yb; the results are shown in Figure 4 at different light intensities. The magnitude of the absorption coefficient is affected by the relative transition strengths. The absorption at $I_c/I_p \sim 1$ is clearly modified when $I \gtrsim I_{sat}$. However, the asymptotic behavior remains the same as the previous calculation.

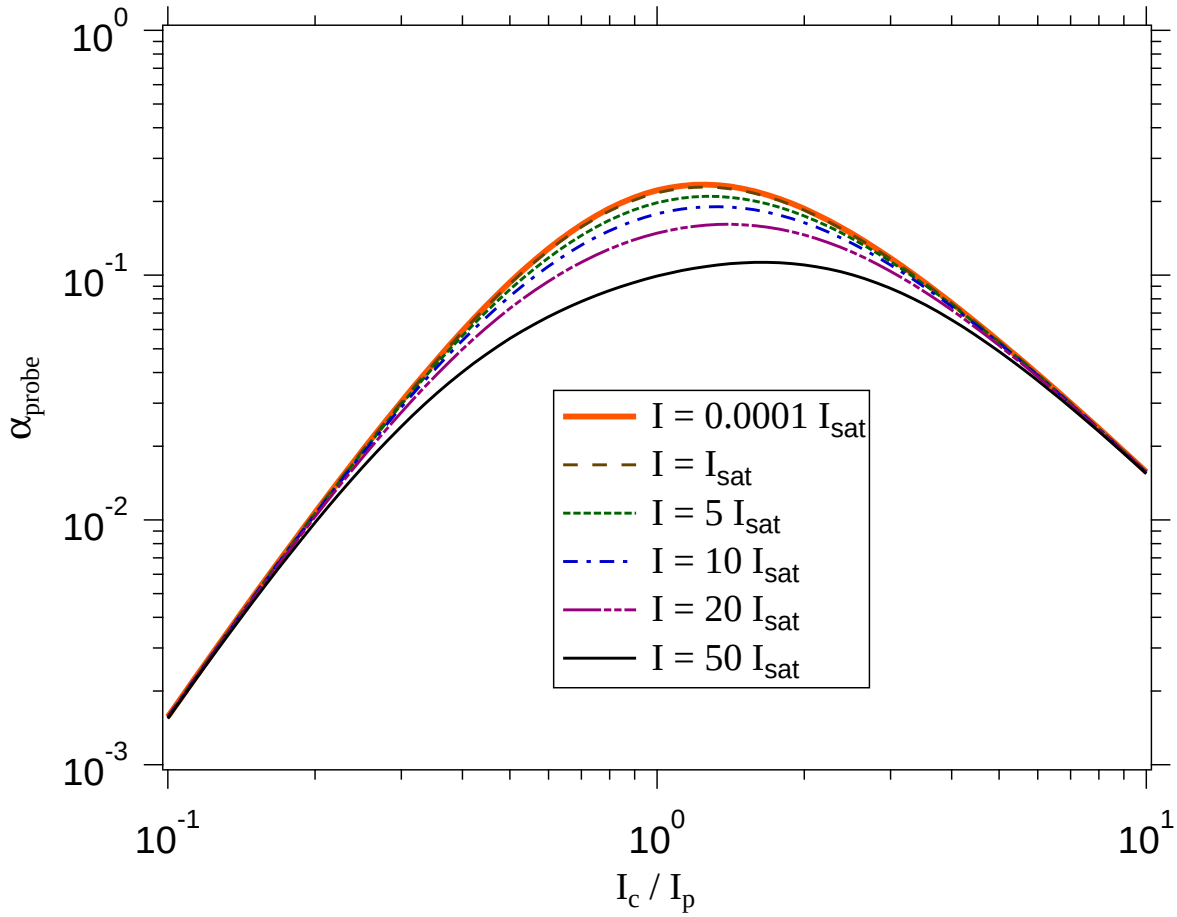

FIG. 4. (Color online) α_{probe} vs. I_c/I_p with different total beam intensity I, showing the saturation effect in a Yb-like $n = 6$ system. The simulation has set $\Delta_1 = \Delta_2 = 0$.

IV. EXPERIMENT

We produce Yb by laser ablation of a solid target, and cool it to 5 Kelvin via cryogenic helium buffer-gas cooling, as described in references [21, 22].

A diagram of the optics setup is shown in Fig. 5. The σ_- control beam and σ_+ probe beams are generated from the same laser beam, and are overlapped and collinear. Their relative power can be adjusted by adjusting the waveplates before the atoms. The control and probe beams have the same frequency and the magnetic field at the atoms is small so as to give near-zero two-photon detuning. We aligned the $\frac{\lambda}{4}$ wave plate and Wollaston prism after the cell so that they separate the control and probe components, which are then detected by PD_c and PD_p photodetectors, respectively. The iris after the cell selects the central area of the EIT beams. By selecting a region of nearly uniform intensity, we reduce complications from averaging over different intensities. A typical power of the laser beam is 0.1 mW with a beam waist of 1.5 mm; a typical iris diameter is 0.9 mm.

In addition to the EIT beams, a weak calibration beam is sent through the cell to measure the optical density in the absence of EIT.

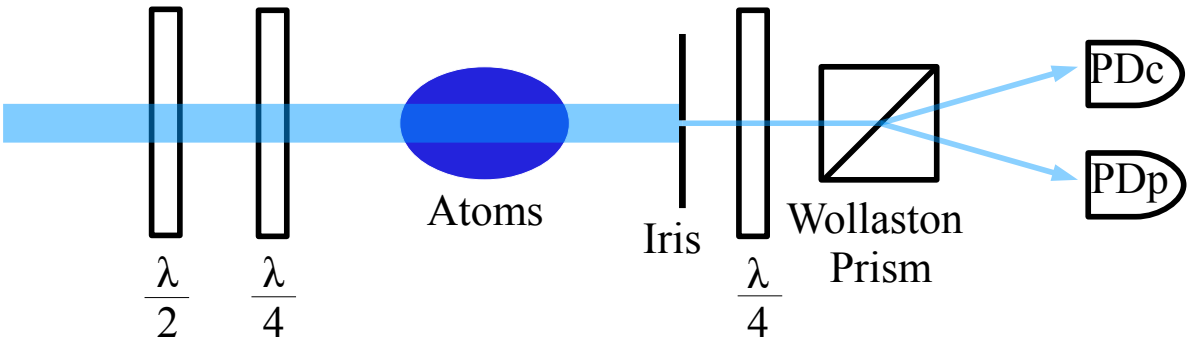

FIG. 5. (Color online) Diagram of optics setup. Not shown is the non-overlapping calibration beam which is sent through the cell to measure the atom density.

A partial spectrum of the ${}^1S_0 \rightarrow {}^1P_1$ transition of Yb is shown in Figure 6. The ^{173}Yb isotope shows good transparency, while the the neighboring $I = 0$ isotopes do not.

To measure the transparency of the ^{173}Yb isotope, we lock the laser so that the EIT beams are tuned to the peak of the $F = 5/2 \rightarrow F' = 5/2$ transition. Our laser is locked via Doppler-free DAVLL spectroscopy of Yb produced in a room-temperature sputtering cell [23]. We simultaneously measure the atomic density in the cell using the calibration beam. The calibration beam is detuned via AOM so that it sits on the side of the ^{174}Yb transition. Because ^{174}Yb is an $I = 0$ isotope, it should not exhibit EIT or optical pumping;

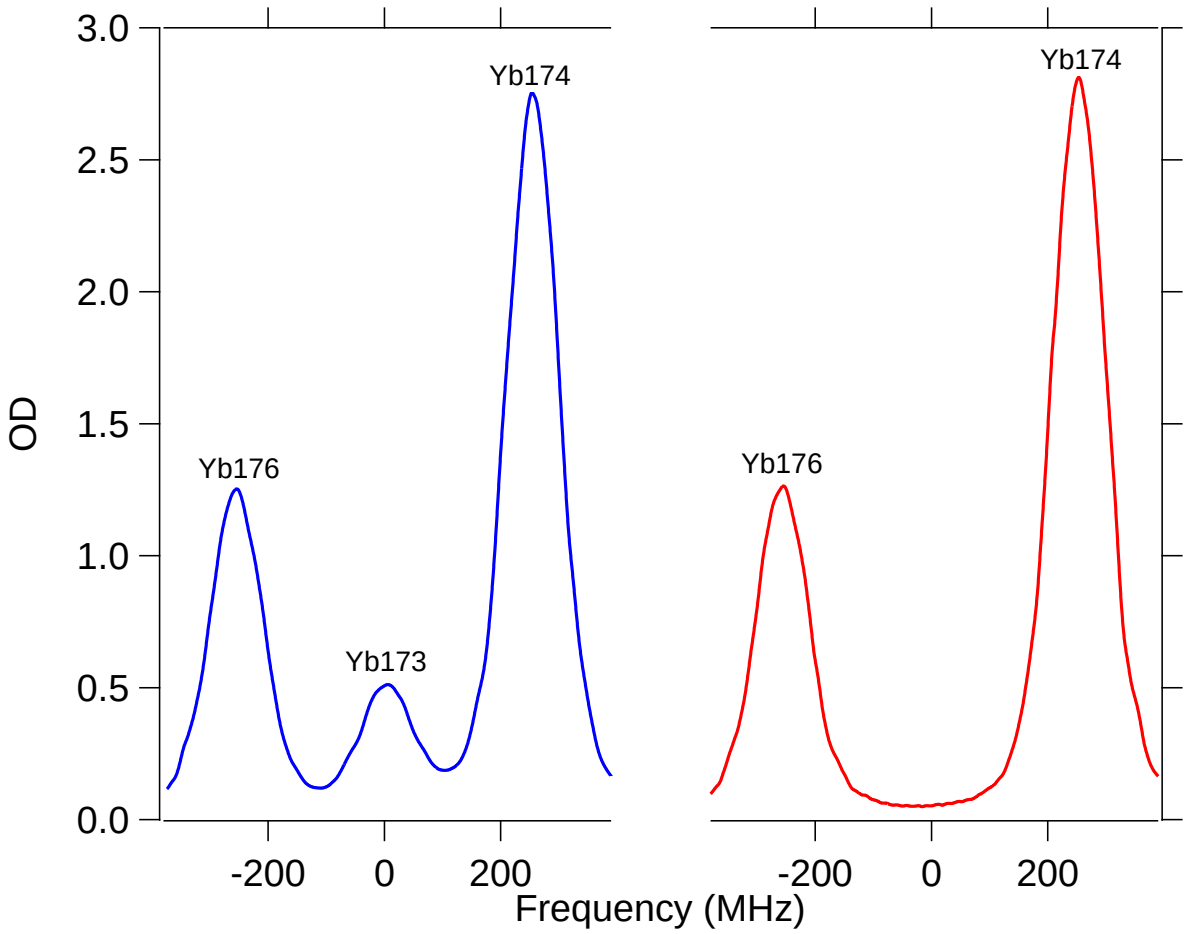

FIG. 6. (Color online) Yb spectra. The blue curve (left) is the spectrum as measured by the calibration beam, the ^{173}Yb transition shown here is the one with $F' = 5/2$, the other two with $F' = 3/2$ and $F' = 7/2$ are not shown here. The red curve (right) is the spectrum of one of the EIT beams. Frequency offset is 25068.2 cm^{-1}.

the detuning from resonance is chosen to give comparable optical densities to those measured by the EIT beams. The intensity of the calibration beam is much smaller than the saturation intensity.

Because the calibration and EIT beams are at different locations in the cell, we must compensate for the different optical paths through the cell. We measure this difference by comparing the optical densities of the ^{176}Yb isotopes as measured by calibration and EIT beams in separate measurements. All measurements are taken at long times after the ablation pulse (approximately 1 second) so that the diffusion of Yb through the cell is well-

described by the lowest-order diffusion mode, and the ratio of densities at the calibration and EIT beam locations does not change in time [24].

Through these measurements, we can calculate the absorption coefficient α relative to α_0, the value of the absorption coefficient in the absence of saturation or EIT. However, at high power ratios, the absorption is dominated by off-resonant absorption from the neighboring $I = 0$ isotopes of Yb, as seen in Figure 6. To compare to the theoretical predictions, we want to subtract off this off-resonance absorption to obtain the contribution to α from ^{173}Yb alone. To do so, we fit the spectrum measured by the calibration beam to a Voight profile to obtain Gaussian and Lorentzian linewidths, and use these linewidths to simulate the off-resonant absorption from the ^{174}Yb and ^{176}Yb. This is subtracted from our data, which is shown in Figure 7.

The vertical error bars result from the combined statistical error of our measurement procedure. The horizontal error bars are obtained from estimates of our systematic error in measurements of the relative beam intensities. The relative intensity is determined from measurements of the beam powers after the Wollaston prism, as shown in Figure 5. Because of birefringence in our cryogenic cell windows (which we estimate to be a retardance of $\lambda/100$), the actual σ_+ and σ_- beam powers can differ from the measured values. The error bars are simulations of the resulting error in measurements of the beam power.

In Figure 7, α/α_0 is shown alongside the calculated values, which are calculated with no free parameters. We note that the data points shows similar transparency for intensity ratios beyond 10; we attribute this to the (fractionally large) errors in intensity and transparency at high intensity ratios. Overall, the data shows good quantitative agreement with theory: the normalized χ^2 is equal to 2. We suspect this slightly high value (dominated by data in the $\frac{I_p}{I_c} = 0.2$ to 0.6 range) is a result of an underestimate of our systematic error in the relative intensities. Evidence for this can be seen in the systematic asymmetry of the data: because of the equivalence of the two EIT beams, the transparency at $\frac{I_p}{I_c} = x$ must be the same as it is at $\frac{I_p}{I_c} = \frac{1}{x}$. Aside from this small discrepancy, we believe the data confirms the predictions of the model.

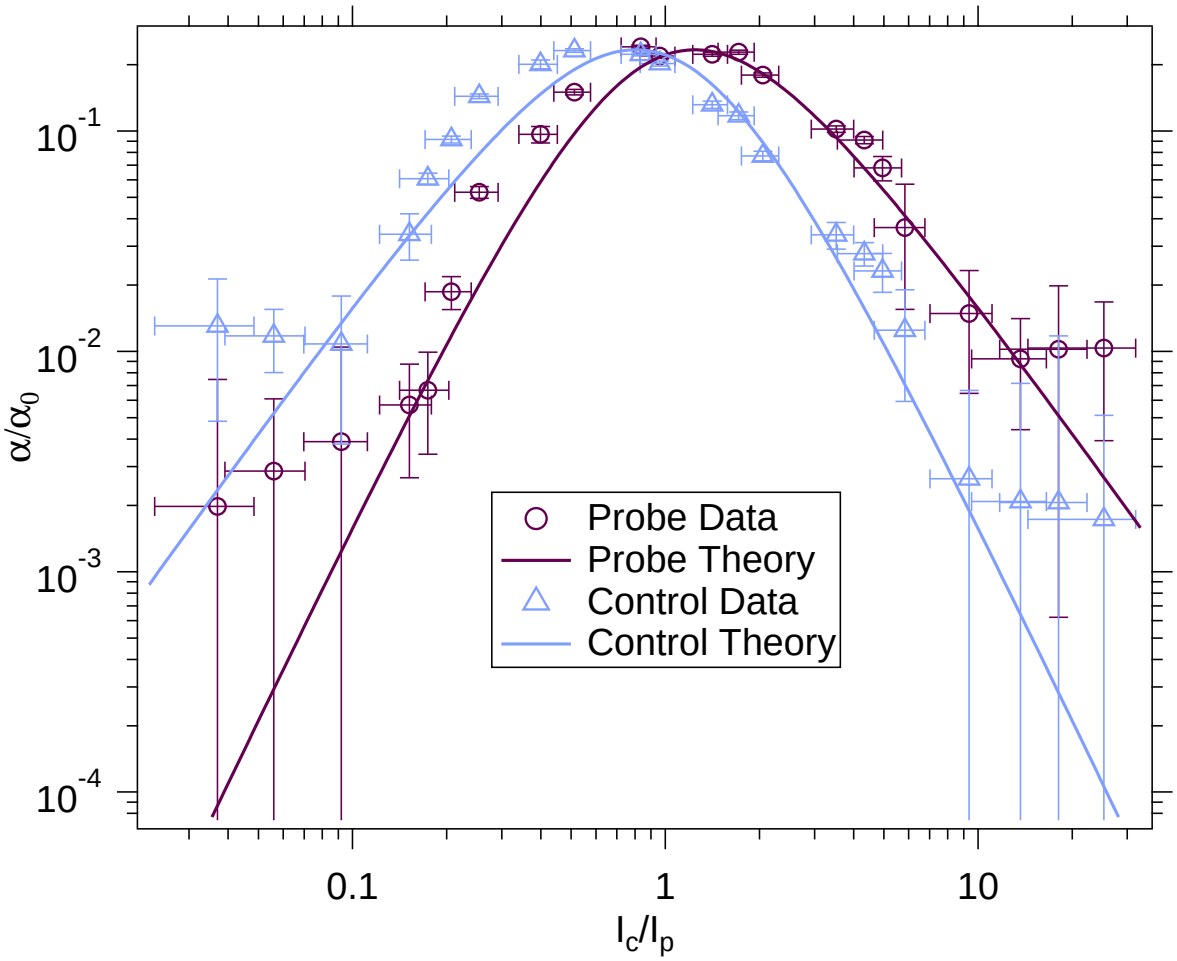

FIG. 7. (Color online) α/α_0 data, as explained in the text. Solid curves are the theoretical models of the control and probe beams for $I/I_{sat} = 0.035$.

V. CONCLUSION / DISCUSSION

Although the open multilevel structure of ^{173}Yb can lead to scattering and a reduction of transparency effect, this can be made arbitrarily small by operating at a sufficiently high intensity ratio. As most quantum information protocols that employ EIT typically operate in this limit, we expect that the open level structure will be of little adverse consequence for experiments employing EIT in ^{173}Yb or other atoms with similar structure.

ACKNOWLEDGEMENTS

Acknowledgements — this material is based upon work supported by the National Science Foundation under Grant No. PHY 0903847.

---

[1] K.-J. Boller, A. Imamolu, and S. E. Harris, Phys. Rev. Lett., **66**, 2593 (1991).

[2] M. Fleischhauer and M. D. Lukin, Phys. Rev. A, **65**, 022314 (2002).

[3] L.-M. Duan, M. D. Lukin, J. I. Cirac, and P. Zoller, Nature, **414**, 413 (2001).

[4] Y.-C. Chen, C.-W. Lin, and I. A. Yu, Phys. Rev. A, **61**, 053805 (2000).

[5] P.-C. Guan, Y.-F. Chen, and I. A. Yu, Phys. Rev. A, **75**, 013812 (2007).

[6] I. Zelensky and V. Mironov, Journal of Experimental and Theoretical Physics, **94**, 916 (2002), ISSN 1063-7761, 10.1134/1.1484987.

[7] A. D. Greentree, D. Richards, J. A. Vaccaro, A. V. Durrant, S. R. d. Echaniz, D. M. Segal, and J. P. Marangos, Phys. Rev. A, **67**, 023818 (2003).

[8] P.-C. Guan and I. A. Yu, Phys. Rev. A, **76**, 033817 (2007).

[9] S. D. Badger, I. G. Hughes, and C. S. Adams, J. Phys. B: At. Mol. Opt. Phys, **34**, L749 (2001).

[10] C. Ottaviani, S. Rebić, D. Vitali, and P. Tombesi, Phys. Rev. A, **73**, 010301 (2006).

[11] X. Liu, L. Kwek, and C. Oh, Laser Physics, **17**, 1089 (2007), ISSN 1054-660X, 10.1134/S1054660X07080130.

[12] A. Kuhn, S. Steuerwald, and K. Bergmann, Eur. Phys. J. D, **1**, 57 (1998).

[13] S. E. Harris and Y. Yamamoto, Phys. Rev. Lett., **81**, 3611 (1998).

[14] M. S. Zubairy, A. B. Matsko, and M. O. Scully, Phys. Rev. A, **65**, 043804 (2002).

[15] C. Hang, Y. Li, L. Ma, and G. Huang, Phys. Rev. A, **74**, 012319 (2006).

[16] D. Das, S. Barthwal, A. Banerjee, and V. Natarajan, Phys. Rev. A, **72**, 032506 (2005).

[17] M.-J. Lu, F. Jose, and J. D. Weinstein, Phys. Rev. A, **82**, 061802 (2010).

[18] M. Fleischhauer, A. Imamoglu, and J. P. Marangos, Reviews of Modern Physics, **77**, 633 (2005).

[19] M. O. Scully and M. S. Zubairy, *Quantum Optics* (Cambridge University Press, 1997).

[20] M. Auzinsh, D. Budker, and S. Rochester, *Optically Polarized Atoms: Understanding light-atom interactions* (Oxford University Press, USA, 2010) ISBN 0199565120.

[21] M.-J. Lu, K. S. Hardman, J. D. Weinstein, and B. Zygelman, Physical Review A (Atomic, Molecular, and Optical Physics), **77**, 060701 (2008).

[22] M.-J. Lu and J. D. Weinstein, Optics Letters, **35**, 622 (2010).

[23] G. Wasik, W. Gawlik, J. Zachorowski, and W. Zawadzki, Applied Physics B: Lasers and Optics, **75**, 613 (2002), ISSN 0946-2171, 10.1007/s00340-002-1041-2.

[24] M.-J. Lu, V. Singh, and J. D. Weinstein, Phys. Rev. A, **79**, 050702 (2009).